03,12

Percolation effect impact on resistive switching of structures based on nanocomposite $(Co_{40}Fe_{40}B_{20})_x(LiNbO_3)_{100-x}$

© K.E. Nikiruy[1], A.V. Emelyanov[1,2,¶], A.N. Matsukatova[1], E.V. Kukueva[1], A.L. Vasiliev[1], A.V. Sitnikov[1,3], V.A. Demin[1], V.V. Rylkov[1,4]

[1] National Research Center „Kurchatov Institute“, Moscow, Russia
[2] Moscow Institute of Physics and Technology (State University), Dolgoprudnyi, Moscow oblast, Russia
[3] Voronezh State Technical University, Voronezh, Russia
[4] Fryazino Branch, Kotel'nikov Institute of Radio Engineering and Electronics, Russian Academy of Sciences, Fryazino, Moscow oblast, Russia

¶ E-mail: emelyanov.andrey@mail.ru

Received June 20, 2022
Revised June 20, 2022
Accepted June 22, 2022

Comparative studies of resistive switching (RS) effect of metal/nanocomposite/metal (M/NC/M), metal/nanocomposite/$LiNbO_3$/metal (M/NC/LNO/M) structures based on NC $(Co_{40}Fe_{40}B_{20})_x(LiNbO_3)_{100-x}$ ($x = 6-20$ at.%) with CoFe nanogranules 2–4 nm in size, as well as structures without a NC layer (M/LNO/M), have been carried out. It was found that the percolation conductivity in NC and presence of a thin LNO layer play a key role in the RS effect. When the metal content approaches the percolation threshold of M/NC/M structures ($x_p \approx 10$ at.%), low-resistance percolation nanochannels of granules are formed in structures with an embedded LNO layer, which ensure their stable RS, which, however, are noticeably suppressed as x decreases relative to x_p by $\Delta x \approx 1-2$ at.%.

Keywords: resistive switching, memristor, nanocomposite, percolation.

DOI: 10.21883/PSS.2022.11.54188.410

1. Introduction

Currently, there is a keen interest in studying metal/dielectric/metal (MDM) memristive structures that demonstrate reversible resistive switching (RS) effects in connection with the prospects of their use to create multilevel memory cells and memristor arrays in matrix implementation, simulating synapses in neuromorphic computer systems aimed at solving artificial intelligence tasks [1–7].

It is essential that these systems often have rich and interesting physical properties attributed, in particular, to the manifestation of interrelated, strongly nonequilibrium processes of thermal, electron, and ion transport on the nanometer scale [8,9], effects of metal nanocrystals nucleation, electrical repolarization of ferroelectric oxide, electron drag of metal atoms (mass-transfer), and conductance quantization in local contractions at room temperatures [10–14].

Recently, we have found and investigated effects of multilevel RS in metal/nanocomposite/metal (M/NC/M) structures based on magnetic NC $(Co_{40}Fe_{40}B_{20})_x(LiNbO_3)_{100-x}$ with CoFe nanogranules and high content of dispersed atoms of Fe and Co in the $LiNbO_3$ isolating matrix (see [15,16] and references therein). High plasticity of the structures (more than 256 RS states) was explained within the well-developed model of the multifilamentary RS mechanism based on the ideas of nucleation of dispersed atoms around percolation chains of nanogranules and formation of low-resistance filamentary nanochannels (filaments) to the „self-organized“ $LiNbO_3$ (LNO) interface layer formed at the bottom electrode of the structures and defining their resistive state. At the same time, the role of the percolation effects remained unstudied. Accordingly, it is not fully clear whether the found RS effects are a property of the used NC or of an amorphous interface LNO interlayer.

In this work, comparative studies are conducted for the NC-based structures $(Co_{40}Fe_{40}B_{20})_x(LiNbO_3)_{100-x}$ with $x = 6-20$ at.% that contain a built-in LNO interlayer (M/NC/LNO/M), without the interlayer (M/NC/M), as well as for the structures without the NC layer (M/LNO/M). It is found that stable and reversible RS arises in the M/NC/LNO/M samples with metal content of $x \approx x_p$, which corresponds to the percolation transition in the M/NC/M structures. At the same time, these structures, as well as the M/LNO/M structures, do not demonstrate stable RS.

2. Samples and experimental methods

The NC-based structures under study $(Co_{40}Fe_{40}B_{20})_x(LiNbO_3)_{100-x}$ were synthesized on

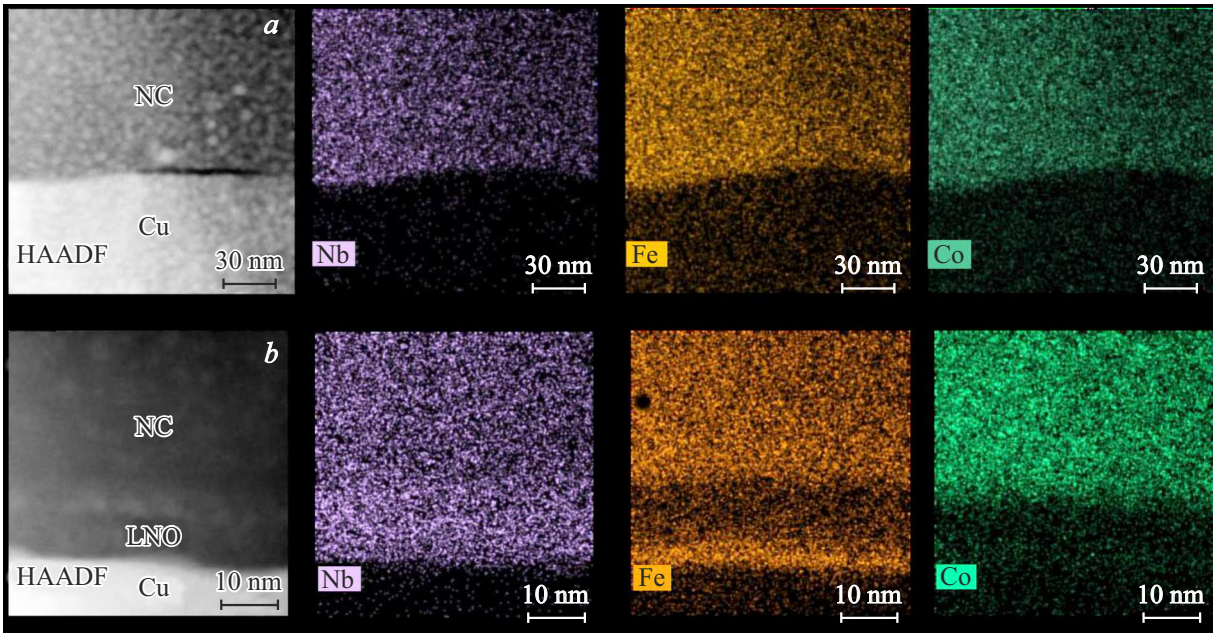

Figure 1. Dark-field TEM image and element distribution maps (Nb, Fe, Co) according to the energy dispersive X-ray microanalysis of the structures: *a* — M/NC/M and *b* — M/NC/LNO/M.

SiO_2/Si substrates by the ion-beam sputtering method using a composite target composed of $Co_{40}Fe_{40}B_{20}$ cast plate and 15 strips of $LiNbO_3$ ferroelectric. An elongated rectangular target was used ($280 \times 80\,mm^2$) with irregular spacing of $LiNbO_3$ ($10 \times 80\,mm^2$) strips, which makes it possible to form the NCs with a different ratio of metal phase in the range of $x = 6-20$ at.% in a single cycle (see [15–17] for details). In the case of M/NC/LNO/M structures, first a layer of $LiNbO_3$ with a thickness of 15 nm was deposited on a substrate, previously coated with Cu film with a thickness of $(0.5-1)\,\mu m$, which acted as the bottom electrode, and then the NC with a technologically set thickness of about 240 nm was deposited through a shadow mask with periodically located holes with a diameter of 5 mm. After that, top Cu electrodes were formed (also through the shadow mask) with a thickness of 500 nm and an area of $0.5 \times 0.2\,mm^2$. Similarly, M/NC/M and M/LNO/M structures were synthesized with an NC layer thickness of ≈ 240 nm and an LNO layer thickness of ≈ 70 nm, respectively.

Microstructure of the prepared samples was studied using the TITAN 80-300 TEM/STEM (FEI, US) transmission electron microscope (TEM) equipped with a high-angle annular dark field (HAADF) detector of electrons (Fischione, USA) and energy-dispersive X-ray spectrometer (EDXS) (EDAX, USA).

The current-voltage curves ($I-V$ curves) of the M/NC/LNO/M structures and their memristive properties were studied at a room temperature using a NI PXIe-4140 multifunctional sourcemeter (National Instruments) and a PM5 (Cascade Microtech) analytic probe station. $I-V$ curves of the M/NC/M structures were measured with grounded bottom electrode and linear sweep of the bias voltage U applied to the top electrode in a sequence from $0 \rightarrow +U_0 \rightarrow -U_0 \rightarrow 0$ V ($U_0 = 5 \cdot 10$ V) with a step of 0.1 V, which can be repeated periodically. Measurements were carried out in an automated mode using the software specially developed in the LabVIEW environment.

Additionally, we have studied the impedance of structures using the Wayne Kerr 6500B precision impedance analyzer in a f frequency range of from 20 Hz to 10 MHz with an alternating signal amplitude of 100 mV.

3. Results and discussion

To study the impact of percolation in NC on the RS effect, comparison studies of the properties of M/NC/LNO/M and M/NC/M structures were carried out. According to the TEM data, as well as the analysis of element distribution by the EDXS method, the M/NC/M structure is a homogeneous layer of nanocomposite material with a thickness of about 260 nm without a self-organized layer of lithium niobate (Fig. 1, *a*). In the M/NC/LNO/M structures with a similar NC thickness, a layer with a reduced content of Co and Fe is clearly seen at the bottom electrode (Fig. 1, *b*).

Typical $I-V$ curves of these structures are shown in Fig. 2. It can be seen that the RS in the structures with a built-in layer of lithium niobate (M/NC/LNO/M) emerges near the percolation threshold of the M/NC/M type structures (for these structures $x_p \sim 9.5-10$ at.%), i.e., under conditions when their $I-V$ curve becomes linear (Fig. 2, *c*).

The multifilamentary RS mechanism in memristive NC structures is based on the nucleation of dispersed atoms

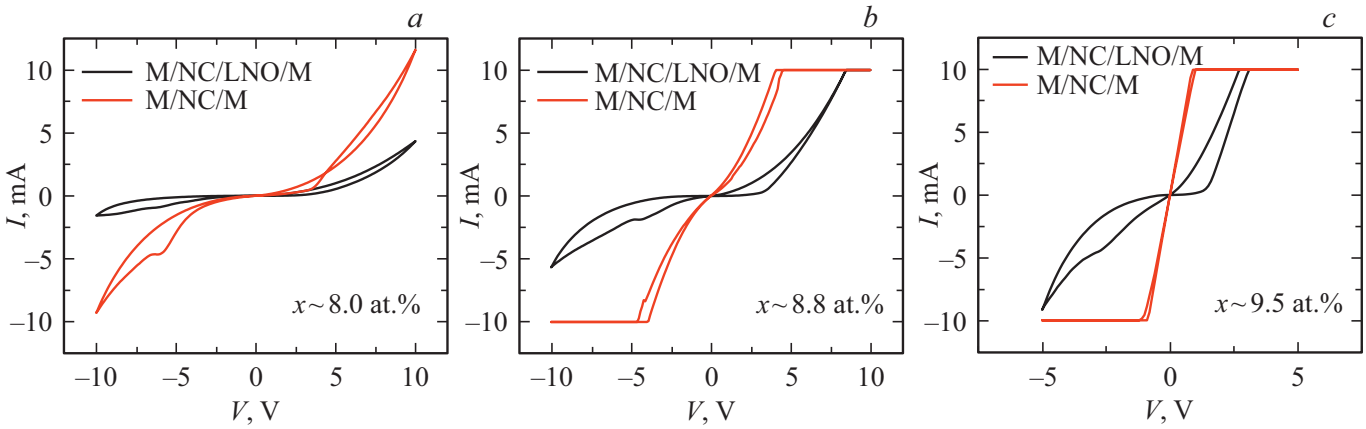

Figure 2. Typical $I-V$ curves of the M/NC/LNO/M (black lines) and the M/NC/M (red lines) structures for different concentrations of metal $x \approx 8.0$ (a), 8.8 (b) and 9.5 at.% (c).

around percolation chains of granules and formation of low-resistance conductive nanochannels (LRCNC) after voltage is applied [15]. When a sufficiently large negative voltage is applied to the top electrode, the structure is switched to a high-resistance state due to the movement of oxygen vacancies and cations to the top electrode via LRCNCs and the increase in the effective gap between them and the bottom electrode. In contrast, when a positive voltage is applied, the structure switches to a low-resistance state due to the migration of vacancies and cations from LRCNCs towards the bottom electrode.

According to the presented data, the number of nucleation centers (metal granules) appears to be insufficient to form low-resistance percolation chains below the percolation threshold (the formed chains are too high-resistance), resulting in the suppression of the multifilamentary RS mechanism (Fig. 2, a). However, when the metal concentration approaches the percolation threshold where $I-V$ curves of the M/NC/M structures become linear (Fig. 2, c), in the M/NC/LNO/M type structures with a built-in layer of lithium niobate low-resistance LRCNCs are formed, which ensures the multifilamentary nature of their RS.

Fig. 3 shows the dependence of an imaginary component of impedance Z'' on the real component Z' for memristive structures with $x \sim 9.5$ at.%, which is a semicircle in the case of the M/NC/LNO/M. Such dependence can be described by an equivalent circuit shown in the inset of Fig. 3 (also, see [14]). This circuit is composed of a parallel R_sC_s circuit and R_c resistance connected in series, which are shunted by the parallelly connected geometric capacitance of the structure modified due to the presence of metal nanoparticles in the dielectric material. R_s resistance and C_s capacitance are connected with the presence of a high-resistance layer of $LiNbO_3$ near the bottom electrode of the structure. R_c resistance, in turn, is defined by the resistance of LRCNC of granulated chains that ensure the contact of the R_sC_s circuit with the top electrode of the structure. Accordingly, in the case of the M/NC/M

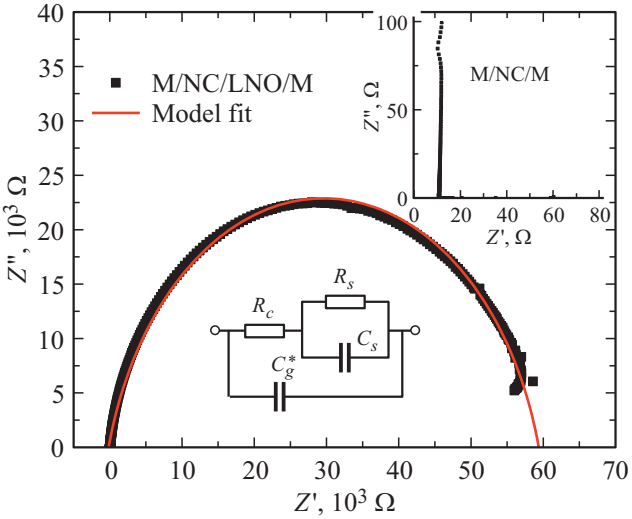

Figure 3. The dependence of imaginary component on real component of impedance (hodograph diagram) for the M/NC/LNO/M structures (black lines) with $x \approx 9.5$ at.% and its approximation according to the circuit shown in the inset (red curve). The right inset shows a hodograph diagram of impedance for the M/NC/M structure with $x \approx 9.5$ at.%.

structures, this circuit degenerates to the resistance of metallized granulated chains $R_c \sim 10\,\Omega$ (inset in Fig. 3).

It is worth noting that for the M/LNO/M structures, as well as for the M/NC/M structures (without a self-organized interlayer), no stable reversible RS was observed. The M/LNO/M structures demonstrate a nonlinear $I-V$ curve (see Fig. 4, a), while the specific resistance in a weak field reaches $\sim 10^9\,\Omega \cdot$ cm, which, probably, corresponds to the hopping mechanism of charge carrier transfer in the amorphous LNO in the impurity band near the Fermi level (specific resistance of the M/NC/M structures reaches $\sim 10^3\,\Omega \cdot$ cm at $x = 9-10$ at.% (Fig. 3, c).

In a strong field, the dependence of conductance on the field follows the $\ln G \propto U^{1/2}$ law (Fig. 4, b), which corre-

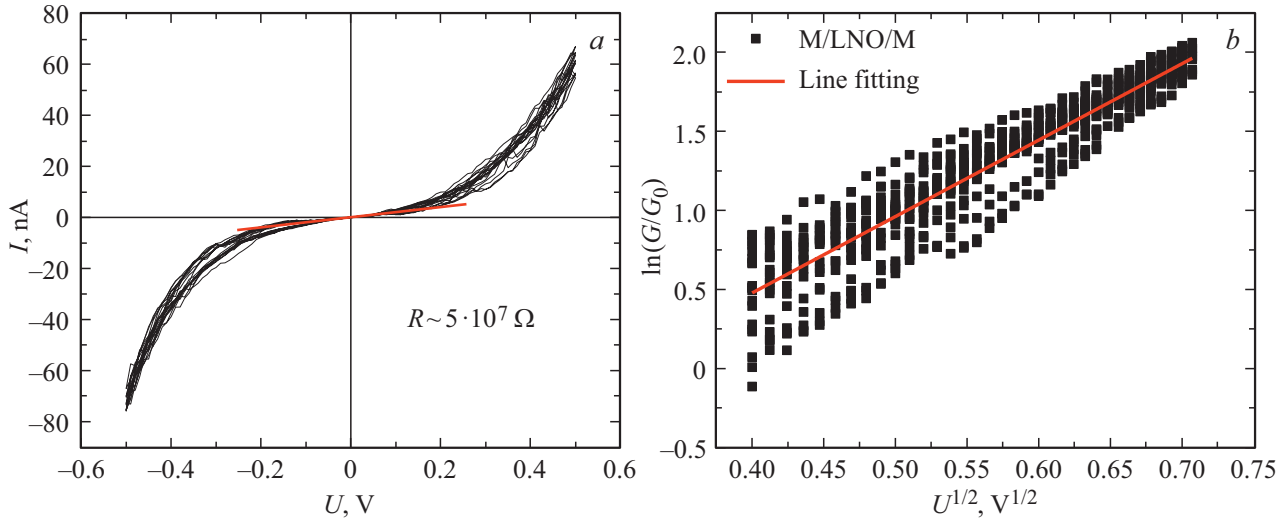

Figure 4. *a* — $I-V$ curve of a M/LNO/M structure with a thickness of $LiNbO_3$ amorphous layer of approx 100 nm. *b* — dependence of admittance logarithm G of this structure on $U^{1/2}$.

sponds to the Frenkel-Poole type mechanism of transfer for thermal-field ionization of isolated Coulomb centers and/or Shklovsky type for the percolation transport of the charge carriers in conditions of strong fluctuation potential [18,19]. Detailed analysis of the hopping transport mechanism in amorphous lithium niobate is of a separate interest and beyond the scope of this study (it requires the thorough study of the $I-V$ curves of the structures at relatively high temperatures [19]).

4. Conclusion

Thus, in this work, we have studied the impact of the percolation effect on RS in the structures based on granulated NC of $(Co_{40}Fe_{40}B_{20})_x(LiNbO_3)_{100-x}$ type. It is shown that in the structures with a built-in layer of lithium niobate of M/NC/LNO/M type stable RS is observed at a metal concentration corresponding to the percolation threshold of the M/NC/M structures, which can be explained within the framework of the recently proposed model of the multifilamentary RS. The equivalent circuit of a memristive cell obtained on the basis of the impedance analysis confirms the presence of a high-resistance interlayer at the bottom electrode of the structure. At the same time, for the structures of the M/LNO/M and M/NC/M type no stable reversible RS was observed, which indicates the key and synergetic role of both the NC layer and the layer of pure oxide (in our case — $LiNbO_3$) in the observation of the RS in granulated structures.

Funding

This research was funded by the Russian Science Foundation (22-19-00171) in part related to the synthesis of the samples and studying of their electrophysical properties, as well as by a grant from the President of the Russian Federation (MK-2203.2021.1.2) in part related to the research of microstructural features of samples.

Measurements were carried out using equipment of the Resource Centers of the NRC „Kurchatov Institute“ (Order No. 2753).

Conflict of interest

The authors declare that they have no conflict of interest.

References

[1] Z. Wang, H. Wu, G.W. Burr, C.S. Hwang, K.L. Wang, Q. Xia, J.J. Yang. Nature Rev. Mater. **5**, 173 (2020).
[2] F. Zahoor, T.Z. Azni Zulkifli, F.A. Khanday. Nanoscale Res. Lett. **15**, 90 (2020).
[3] W. Huang, X. Xia, C. Zhu, P. Steichen, W. Quan, W.i Mao, J. Yang, L. Chu, X. Li. Nano-Micro Lett. **13**, 85 (2021).
[4] A.V. Emelyanov, K.E. Nikiruy, A.V. Serenko, A.V. Sitnikov, M.Yu. Presnyakov, R.B. Rybka, A.G. Sboev, V.V. Rylkov, P.K. Kashkarov, M.V. Kovalchuk, V.A. Demin. Nanotechnology **31**, 045201 (2020).
[5] V.A. Demin, D.V. Nekhaev, I.A. Surazhevsky, K.E. Nikiruy, A.V. Emelyanov, S.N. Nikolaev, V.V. Rylkov, M.V. Kovalchuk. Neural Networks **134**, 64 (2021).
[6] M. Zhuk, S. Zarubin, I. Karateev, Yu. Matveyev, E. Gornev, G. Krasnikov, D. Negrov, A. Zenkevich. Front. Neurosci. **14**, 94 (2020).
[7] S. Shchanikov, A. Zuev, I. Bordanov, S. Danilin, V. Lukoyanov, D. Korolev, A. Belov, Y. Pigareva, A. Gladkov, A. Pimashkin, A. Mikhaylov, V. Kazantsev, A. Serb. Solitons Fractals **142**, 110504 (2021).
[8] J.S. Lee, S. Lee, T.W. Noh. Appl. Phys. Rev. **2**, 031303 (2015).
[9] A.N. Matsukatova, A.V. Emelyanov, A.A. Minnekhanov, V.A. Demin, V.V. Rylkov, P.A. Forsh, P.K. Kashkarov. Pis'ma v ZhETF **112**, 379 (2020) (in Russian).

[10] A. Mikhaylov, A. Belov, D. Korolev, I. Antonov, V. Kotomina, A. Kotina, E. Gryaznov, A. Sharapov, M. Koryazhkina, R. Kryukov, S. Zubkov, A. Sushkov, D. Pavlov, S. Tikhov, O. Morozov, D. Tetelbaum. Adv. Mater. Technol. **5**, 1900607 (2019).
[11] V. Mikheev, A. Chouprik, Yu. Lebedinskii, S. Zarubin, A.M. Markeev, A.V. Zenkevich, D. Negrov. Nanotechnology **31**, 215205 (2020).
[12] A.S. Vedeneev, V.V. Rylkov, K.S. Napol'sky, A.P. Leont'ev, A.A. Klimenko, A.M. Kozlov, V.A. Luzanov, S.N. Nikolaev, M.P. Temiryazeva, A.S. Bugaev. Pis'ma v ZhETF **106**, *6*, 387 (2017) (in Russian).
[13] O.G. Kharlanov, B.S. Shvetsov, V.V. Rylkov, A.A. Minnekhanov. Phys. Rev. Appl. **17**, 054035(17) (2022).
[14] G. Milano, M. Aono, L. Boarino, U. Celano, T. Hasegawa, M. Kozicki, S. Majumdar, M. Menghini, E. Miranda, C. Ricciardi, S. Tappertzhofen, K. Terabe, I. Valov. Adv. Mater. (2022). https://doi.org/10.1002/adma.202201248
[15] M.N. Martyshov, A.V. Emelyanov, V.A. Demin, K.E. Nikiruy, A.A. Minnekhanov, S.N. Nikolaev, A.N. Taldenkov, A.V. Ovcharov, M.Yu. Presnyakov, A.V. Sitnikov, A.L. Vasiliev, P.A. Forsh, A.B. Granovskiy, P.K. Kashkarov, M.V. Kovalchuk, V.V. Rylkov. Phys. Rev. Appl. **14**, 034016 (2020).
[16] V.V. Rylkov, A.V. Emelyanov, S.N. Nikolaev, K.E. Nikiruy, A.V. Sitnikov, E.A. Fadeev, V.A. Demin, A.B. Granovsky. ZhETF **158**, *1*(*7*), 164 (2020) (in Russian).
[17] V.V. Rylkov, S.N. Nikolaev, V.A. Demin, A.V. Emelyanov, A.V. Sitnikov, K.E. Nikiruy, V.A. Levanov, M.Yu. Presnyakov, A.N. Taldenkov, A.L. Vasil'ev, K.Yu. Chernoglazov, A.S. Vedeneev, Yu.E. Kalinin, A.B. Granovsky, V.V. Tugushev, A.S. Bugaev. ZhETF **153**, 424 (2018) (in Russian).
[18] B.A. Aronzon, D.Yu. Kovalyov, V.V. Rylkov. FTP **39**, 844 (2005) (in Russian).
[19] A.A. Gismatulin, V.N. Kruchinin, V.A. Gritsenko, I.P. Prosvirin, T.-J. Yen, A. Chin. Appl. Phys. Lett. **114**, 033503 (2019).